Optical Materials: X 15 (2022) 100164

Contents lists available at ScienceDirect

Optical Materials: X

journal homepage: www.journals.elsevier.com/optical-materials-x

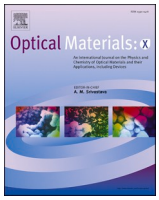

Invited Article

(INVITED)Transparent Er^{3+} doped Ag_2O containing tellurite glass-ceramics☆

I. Aromäki [a], I. Shestopalova [a], R. Ponte [a], S. Annurakshita [a], G. Bautista [a], A. Othmani [b], H. Elhouichet [c,d], L. Petit [a,*]

[a] Photonics Laboratory, Tampere University, FI-33101, Tampere, Finland
[b] Laboratoire de Physique des Matériaux, Faculté des Sciences de Bizerte, Université de Carthage, 7021, Zarzouna, Tunisia
[c] Physics Department, College of Sciences, University of Bisha, B.P. 551, Bisha, 61922, Saudi Arabia
[d] Sciences Faculty of Tunis, University of Tunis El Manar, 2092, Tunisia

A B S T R A C T

Transparent Er^{3+} doped Ag_2O containing tellurite glass-ceramics were fabricated by melting process followed by a heat treatment at 20 °C above the glass transition temperature of the glass for 2 to 17 h. The effects of the crystallization on the optical and luminescence properties of the glasses are presented and discussed. The precipitation of Bi_4TeO_8 crystal was confirmed in all the glasses, independently of their composition. From the spectroscopic properties, the heat treatment was found to have no impact on the site of the Er^{3+} ions indicating that the Er^{3+} ions remain in the amorphous part of the glass-ceramic. Although Ag nanoparticles could be evidenced using transmission electron microscopy and nonlinear optical imaging, no surface plasmon resonance band of Ag nanoparticles appeared in the absorption spectrum of the heat treated glasses. No enhancement of the NIR emission centered at 1.5 μm was observed probably due to the low concentration of Ag nanoparticles precipitating in the glasses. However, an increase in the intensity of the upconversion and mid-infrared emissions was observed from the glass-ceramics prepared with the low amount of Ag_2O (<1 mol%). As evidenced using Raman spectroscopy, the addition of Ag_2O was found to depolymerize the tellurite network. The precipitation of the Bi_4TeO_8 crystal in the most polymerized glasses is suspected to reduce the Er–Er distances whereas it has no significant impact on the Er–Er distances in glasses with a depolymerized network.

1. Introduction

Since the discovery of the single-mode Nd^{3+} doped tellurite fiber laser in 1994 [1] and of the broadband Er^{3+} doped tellurite fiber amplifier in 1997 [2], tellurite glasses have attracted a lot of attention due to their good network forming capability and their good physical and chemical stability. Additionally, they possess low phonon energy (~750 cm^{-1}) and high linear and nonlinear refractive indices [3]. Compared to silica and silicate glasses, tellurite glasses have lower melting temperature and enable higher solubility of rare-earth (RE) ions so that the luminescence quenching phenomenon occurs at high RE concentrations [4]. Due to their emission band with large bandwidth and high emission cross-section when doped with RE ions (especially Er^{3+} ions), these glasses are considered as good materials for ultra-broadband fiber amplification [5]. Er^{3+} doped zinc-tellurite glasses were developed with upconversion (UC) emissions in the visible range and also downconversion emissions in the near- (NIR) and mid-infrared (MIR) (1.5 and 2.7 μm, respectively) [6], which are useful for modern lighting devices and optical displays, for example [7].

It is well known that the spectroscopic properties of RE doped glasses can be enhanced using metal nanoparticles (NPs) due to their optical responses that are governed mainly by the surface plasmon resonance (SPR) [8]. Significant enhancement in the spectroscopic properties of Er^{3+} doped tellurite glass due to silver NPs was reported in Ref. [9] and was related to the strong local electric field induced by SPR of Ag NPs and also by energy transfer from the surface of silver NPs to Er^{3+} ions.

Since the discovery of the first GC in 1960 by Stookey [10], glass-ceramics (GCs) have been materials of interest. GC is a material that contains at least one type of functional crystalline phase and a residual glass [11]. GCs are usually obtained by heat-treating a glass under specific heating conditions to form nuclei and grow them into crystals. GC can exhibit enhanced spectroscopic properties such as higher absorption and emission cross-sections compared to the parent glass when the RE ions are located in the crystalline phases with appropriate

☆ Given her role as Associate Editor of this journal, Laeticia Petit had no involvement in the peer-review of articles for which he was an author and had no access to the information regarding their peer-review. Full responsibility of the per-review process for this article was delegated to another Editor.

* Corresponding author.
E-mail address: laeticia.petit@tuni.fi (L. Petit).

https://doi.org/10.1016/j.omx.2022.100164
Received 26 April 2022; Received in revised form 31 May 2022; Accepted 2 June 2022
Available online 16 June 2022

crystalline phase. For many photonics applications, the GC should be transparent. In this case, the crystals should be homogeneously distributed in the volume of the glass. To minimize light scattering, the crystals should have a size smaller than the incident light wavelength (typically <50–100 nm) [12] and also a similar refractive index to the host glass [13]. Since the first demonstration of the transparent Er^{3+}, Yb^{3+} codoped GCs [4], effort has been made on the development of new transparent GCs, especially within the tellurite glass system [14–17]. In our previous study, we investigated the nucleation and growth process of tellurite glasses in the TeO_2–Bi_2O_3–ZnO system [18] and the glass with the $70TeO_2$–$10Bi_2O_3$–20ZnO composition (in mol%) was found to be a promising glass for the preparation of transparent GC as crystals such as $Bi_2Te_4O_{11}$ precipitate in the volume of the glass.

Here, Er^{3+} doped glasses with the $70TeO_2$–$10Bi_2O_3$–20ZnO composition (in mol%) were prepared with Ag_2O to understand the impact of the glass composition on the formation of transparent GCs. First, the impact of the addition of Ag_2O on the physical, thermal, optical, structural and luminescence properties are discussed. Then, the results on the preparation and characterization of the transparent GCs are presented.

2. Experimental procedure

Glasses with the composition $(97.5 - x)\ (0.70TeO_2 - 0.20ZnO - 0.10Bi_2O_3) - x\ Ag_2O - 2.5Er_2O_3$ with x = 0, 0.5, 1, 2 and 4 (in mol %) were prepared using the standard melting quenching technique. The glasses are labeled as Agx. TeO_2 (Alfa Aesar, ≥ 99%), ZnO (Aldrich, 99.99%), Bi_2O_3 (Aldrich, 99.9%), Er_2O_3 (Aldrich, ≥ 99.99%) and Ag_2SO_4 (Sigma-Aldrich, ≥ 99.5%) were used as the raw materials. The ~20 g batches were melted in a quartz crucible at 775 °C for 40 min. After quenching, the glasses were annealed at 200 °C, well below their respective glass transition temperature (T_g), for 6 h, which was efficient to release the stress from the quench. Finally, the polished glasses were heat treated at T_g + 20 °C for 2–17 h.

The thermal properties of the glasses were measured using a NETZSCH STA 449 F1 Differential Scanning Calorimetry (DSC). A heating rate of 10 °C/min was used. The T_g was taken at the inflection point of the first endothermic signal and the crystallization temperature (T_p) at the exothermic peak maximum. The onset of crystallization (T_x) was obtained at the intersection of the tangent of the exotherm peak with the baseline. The thermal properties of the glasses are given at ± 3 °C.

The density (ρ) was measured with an accuracy of ±0.02 g/cm^3 using the Archimedes principle. Ethanol was used as the immersion liquid.

The crystalline phase of the GCs after heat treatment was determined using a Panalytical EMPYREAN multipurpose X-Ray Diffractometer (XRD). A Ni filtered Cu-Kα radiation was used and the diffractograms were acquired at rotation angles (2θ) from 15° to 60°, with a step of 0.013°.

Carl Zeiss Crossbeam 540 Gemini scanning electron microscope (SEM) with an Energy Dispersive X-ray Spectroscopy (EDS) detector (X-MaxN 80) was used to image and analyze the surface of the as prepared and heat treated glasses, which were polished and coated with a conductive carbon layer.

The absorption spectra were measured from polished samples using a UV-VIS-Near-IR Spectrophotometer (UV-3600 Plus, Shimadzu). The absorption cross-sections were calculated using Eq. (1).

$$\sigma_{abs}(\lambda) = \frac{\ln 10 \log(\frac{I}{I_0})}{NL} \quad (1)$$

where N is the concentration of RE ions per cm^3, L the thickness of the glass (cm) and $\log(\frac{I}{I_0})$ is the absorbance. The accuracy is ±10%.

The refractive index (n) of the glasses was measured at different wavelengths using 10 scans by the prism coupling technique using Metricon (model 2010) which also provides the fitting of the experimental refractive index data using Sellmeier equation [19]:

$$n(\lambda) = a + \frac{b}{\lambda^2} + \frac{c}{\lambda^4} \quad (2)$$

where λ is the wavelength. a, b and c are the experimentally determined Sellmeier coefficients. The estimated error of the n measurement was ±0.001.

The upconversion (UC) spectra of the glasses were obtained using a TEC-cooled fiber-coupled multimode laser (II-VI Laser enterprise), with excitation wavelength (λ_{exc}) ~ 975 nm, reaching the surface with a power of approximately 400 mW and a Spectro 320 optical spectrum analyzer (Instrument Systems Optische Messtechnik GmbH, Germany). The NIR and MIR emission spectra in the 1425-1675 nm range and in the 2500–3000 nm range, respectively, were measured using an extended IR photomultiplier (Hamamatsu H10330A-75) and using a monochromator coupled with an amplified MIR detector (detector PCI-4TE-4-1x1, preamplifier PIP-DC-200M-F-M4, Vigo), respectively. All the emissions spectra were collected at room temperature.

Cut and polished heat treated glass samples (Ag0 and Ag4) were imaged using a custom-built nonlinear optical (NLO) scanning microscope. The microscope was composed of a femtosecond laser (wavelength of 1060 nm, pulse length of 140 fs, repetition rate of 80 MHz), microscope objective (magnification of 50x, numerical aperture of 0.8), three-dimensional (3D) piezo-based scanning system, cooled photomultiplier tube, relay lenses and mirrors, and appropriate optical filters. To acquire a NLO scanning map, the nonlinear signals from the sample were collected in back-reflection mode and point-by-point, i.e., as a function of the relative position of the sample with respect to the focal region of the incident laser beam. Microscopic regions (20 μm by 20 μm) of interest in each glass sample were scanned at 100 by 100 pixels resolution. Using appropriate bandpass filters (320 ± 20 nm, 356 ± 15 nm, 385 ± 13 nm, 500 ± 7.5 nm, 532 ± 9 nm and 560 ± 7 nm) placed before the photomultiplier tube, the spectrally resolved third-harmonic, second-harmonic and nonlinear luminescence signals from the samples were obtained. The incident polarization used was along the vertical direction. The average input power used was 5 mW, and the pixel dwell time was 50 ms. All NLO experiments were performed at room temperature.

A transmission electron microscope (TEM 2100, JEOL) with a resolution of 0.2 nm and voltage acceleration of 200 kV was used to obtain the microstructure and to verify the existence of crystallized phases in the glassy host. The fine powder of glass was dispersed in acetone and isolated by an ultrasonic bath for about 20 min. A drop of solution was spatted on the copper grid and dried before analysis.

3. Results and discussion

Er^{3+} doped tellurite glasses within the TeO_2–ZnO–Bi_2O_3–Ag_2O system were prepared and characterized to understand the impact of the glass composition on the formation of transparent GCs. The density and thermal properties of the glasses are summarized in Table 1. The values are found to be similar to those reported by Massera et al. [18]. An increase in the Ag_2O content (x) decreases the T_g and also the density which is due to the replacement of Te and Bi with high atomic mass by Ag. The progressive addition of Ag_2O also shifts T_p to higher

Table 1
Density and characteristic temperatures of the investigated glasses.

Glass	T_g (°C) ±3 °C	T_x (°C) ±3 °C	T_p (°C) ±3 °C	ΔT = T_x - T_g ±6 °C	ρ (g/cm^3) ±0.02 g/cm^3
Ag0	353	434	446	81	6.20
Ag0.5	352	436	448	84	6.19
Ag1	349	434	448	85	6.18
Ag2	342	436	455	94	6.17
Ag4	332	444	473	112	6.15

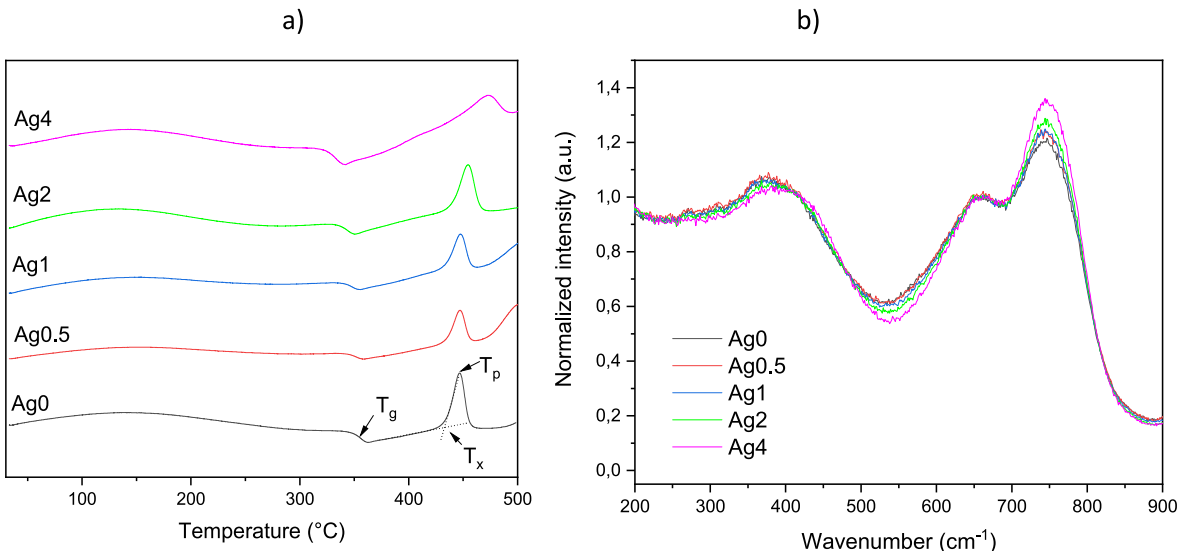

Fig. 1. Thermogram (a) and normalized Raman spectra (b) of the investigated glasses (Agx).

temperature. As a consequence, ΔT increases indicating that the addition of Ag_2O increases the resistance of the glass toward crystallization [20]. As seen in Fig. 1a, the shape of the crystallization peak becomes broader and less intense as x increases indicating a decrease in the crystallization tendency of the glasses when adding Ag_2O in the tellurite glass. The decrease in the density and in T_g can be also related to structural modifications that occur with the insertion of Ag_2O as evidenced by the Raman spectra of the glasses (Fig. 1b). The spectra exhibit a band at ~370 cm^{-1} which can be related to Zn–O [21] and Bi–O–Bi vibrations [22], the intensity of this bans slightly decreasing as x increases due to the replacement of ZnO and Bi_2O_3 by Ag_2O. The shoulder at ~450 cm^{-1} can be related to highly coupled bending and stretching modes of chains Te–O–Te of corner sharing TeO_4, TeO_{3+1} and TeO_3 units [Guery]. The band at 660 cm^{-1} is related to stretching of Te–O bond in [TeO_4] trigonal bipyramidal units or to [Te–O–Te] linkage between two fourfold-coordinated Te atoms, whereas the band at ~750 cm^{-1} belongs to the stretching vibration modes between Te and non-bridging oxygen (NBO) atoms in disordered TeO_3 and/or TeO_{3+1} units, in which one Te–O bond is lengthened [G]. As the concentration of Ag_2O increases, the intensity of the band at 750 cm^{-1} increases compared to that of the band at 660 cm^{-1}. This reveals a progressive depolymerization of the tellurite network with an increase in the distorted TeO_3 units at the expense of TeO_4 units which is in agreement with the decrease in $T_{g\ as\ x}$ increases (Table 1). The depolymerization of the tellurite network is also evidenced by the increase in intensity and the shift to higher wavenumber of the shoulder at 450 cm^{-1} [23]. Similar impact of the addition of Ag_2O on the structural and thermal properties of tellurite glasses was reported by Bachvarova-Nedelcheva et al. [24].

The absorption spectra of the glasses are presented in Fig. 2a. The spectra exhibit the typical absorption bands related to the Er^{3+} ions 4f-4f transitions from the ground state to various excited levels. No changes in the position of the band gap nor in the shape and intensity of the absorption bands with an increase in x can be seen (Fig. 2b and c). One should point out that the spectra do not exhibit the silver surface plasmon resonance (SPR) band usually at around 450 nm indicating that silver is possibly in its ionic forms in the glass. From the absorption coefficient, the absorption cross-sections were measured using Eq. (1). The absorption cross-sections at 975 and 1532 nm are, respectively, (3.4×10^{-21}) cm^2 and (8.1×10^{-21}) cm^2 (at ± 10%), independently of x and are similar to the absorption cross-sections reported for other tellurites glasses [25,26]. Thus, although the addition of Ag_2O modifies the structure of the glass, the sites of the Er^{3+} ions are expected to be similar in all the investigated glasses.

The refractive indices of the glasses were measured at different wavelengths. As depicted in Fig. 2d, the refractive index of the investigated tellurite glasses is higher than the refractive index of silica glass for example [27] due to the high polarization of the TeO_2 network [28] but similar to those reported for tellurite glasses (over 2.1 at 444 nm) [29]. An increase in the Ag_2O decreases n in agreement with the decrease in the density of the glass as x increases. Fig. 2e depicts the well-known absorption band related to the free, weakly associated hydroxyl (OH) groups (band at around 3250 cm^{-1}) and to the strongly associated OH groups (shoulder at 2800 cm^{-1}) [30]. Despite their different glass structure, the investigated glasses have similar content of OH groups.

The glasses exhibit similar shape of emissions at 2.7 μm, 1.5 μm and in the visible after 980 nm pumping as depicted in Fig. 3a, b and c, respectively. The emission at 2.7 μm is due to the $^4I_{11/2} \rightarrow {}^4I_{13/2}$ transition. Due to the large concentration of Er_2O_3 in the glasses, the Er–Er distances are expected to be short benefiting the emission at 2.7 μm from the energy transfer upconversion (ETU) between neighboring Er^{3+} ions: $^4I_{13/2} + {}^4I_{13/2} \rightarrow {}^4I_{9/2} + {}^4I_{15/2}$ [31]. The emission band at 1.5 μm is due to the $^4I_{13/2} \rightarrow {}^4I_{15/2}$ transition of Er^{3+} ions. The green and red emissions are assigned to $^2H_{11/2}$, $^4S_{3/2} \rightarrow {}^4I_{15/2}$ and $^4F_{9/2} \rightarrow {}^4I_{15/2}$ transitions of Er^{3+} ions, respectively [6]. These broad emission bands are typical emissions from Er^{3+} ions located in tellurite glasses [32]. Within 10%, all glasses exhibit similar intensity of the NIR emission. However, as shown in Fig. 4a and b, an increase in x decreases the intensity of the emissions at 2.7 μm and of the upconversion (UC) emissions. As the glasses have similar absorption cross-section at 980 nm and similar content of OH groups, the addition of Ag_2O is thus believed to change the Er^{3+} ions solubility in the glasses as it leads to different network connectivity as discussed in the previous section. The depolymerization of the tellurite network induced by the addition of Ag_2O is thought to increase the distances between the Er^{3+} ions and as a consequence to decrease the intensity of the (green and red) UC and MIR emissions. A better solubility of the Er^{3+} ions in the tellurite network is, thus, suspected when adding Ag_2O.

The glasses were heat treated at their respective (T_g + 20 °C) for 2–17 h. The glasses heat treated for 17 h are opaque (Fig. 5a), the highly Ag concentrated glasses being still slightly translucent after the heat treatment for 17 h confirming that the addition of the Ag_2O in the tellurite glass reduces the tendency of the glass to crystallization and especially its rate of crystallization as discussed earlier. Fig. 6 presents the XRD pattern of the glasses prior to and after heat treatment. Sharp peaks can be seen in the XRD patterns of all the heat-treated glasses and

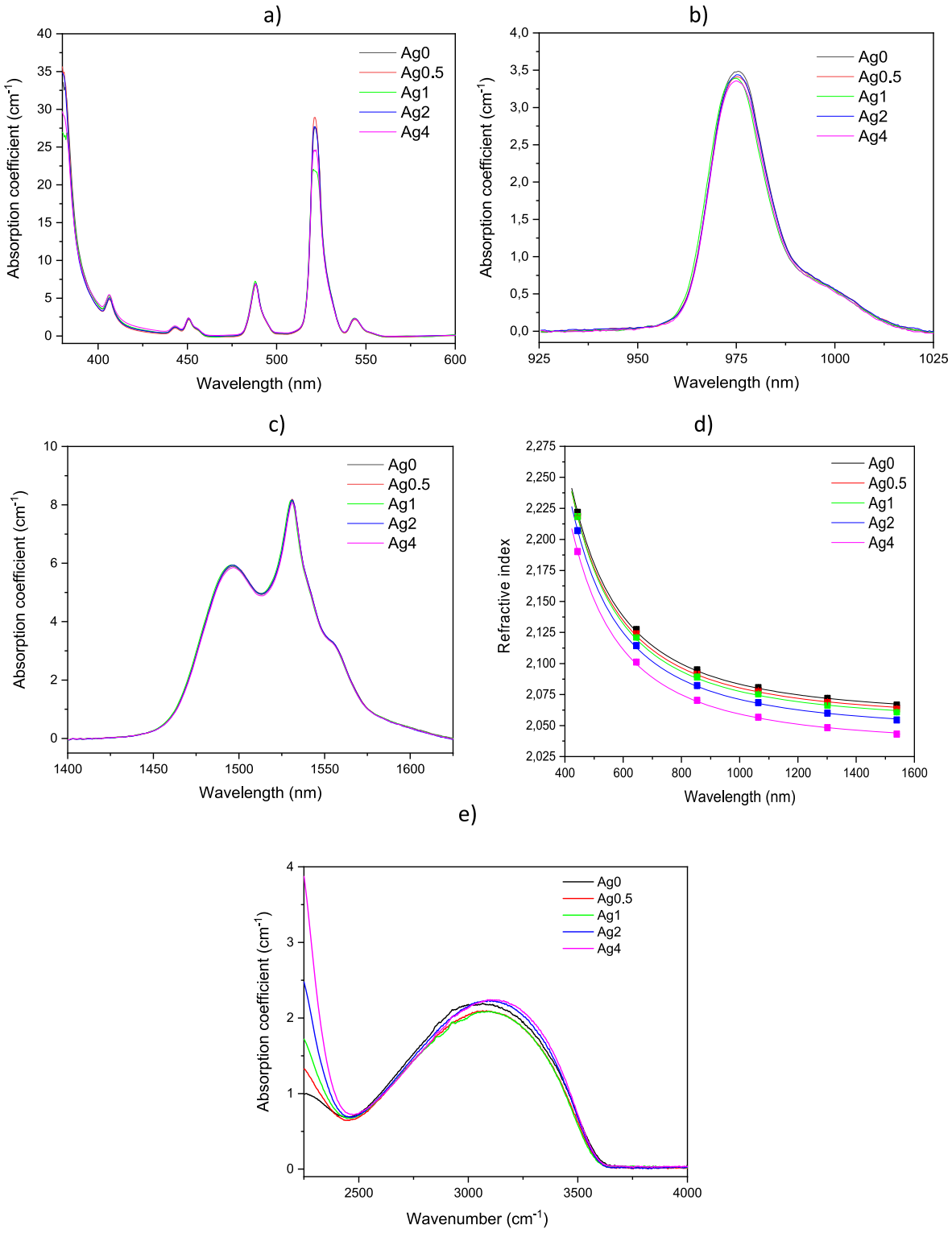

Fig. 2. Absorption spectra (a), absorption bands centered at 975 nm (b) and at 1531 nm (c) and refractive indices (d) of the investigated glasses. The refractive indices were measured at 6 different wavelengths and fitted with the Sellmeier formula. The filled squares represent the experimental data, while the continuous lines are the fitting curves. IR absorption spectra of the glasses (e).

they correspond to Bi_4TeO_8 crystal (ICDD 00-024-0157). Thus, the addition of Ag_2O does not have an impact on the crystallization process in the tellurite glass. Similar crystal was reported to precipitate in undoped glass within similar system [18]. However, the first phase to precipitate in the undoped glass was reported to be the Bi_2O_3 crystal. Higher temperature was needed to precipitate the Bi_4TeO_{11} crystal. Here, the investigated glasses contain Er and Ag. They were prepared in quartz crucible whereas the glasses from Ref. [18] were prepared in Pt crucible. According to the EDS analysis, the investigated glasses contain Si due to the contamination from the quartz crucible. Therefore, the addition of Er, Ag and Si in the tellurite glass seems to promote the precipitation of Bi_4TeO_8 crystal the expense of Bi_2O_3. Additionally, the

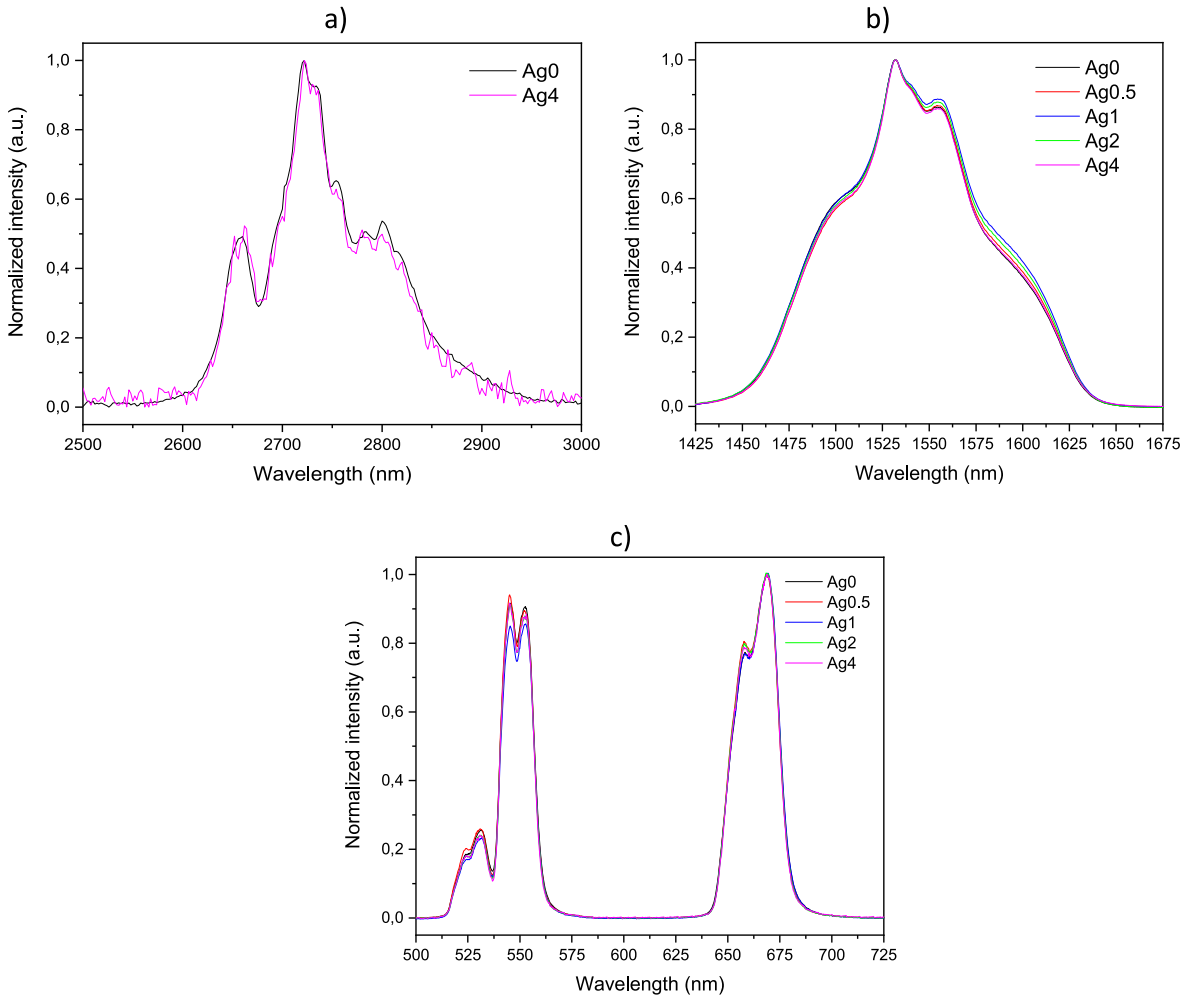

Fig. 3. Normalized emission spectra centered at 2.7 μm (a) and at 1.5 μm (b) and normalized upconversion spectra (c) of the investigated glasses.

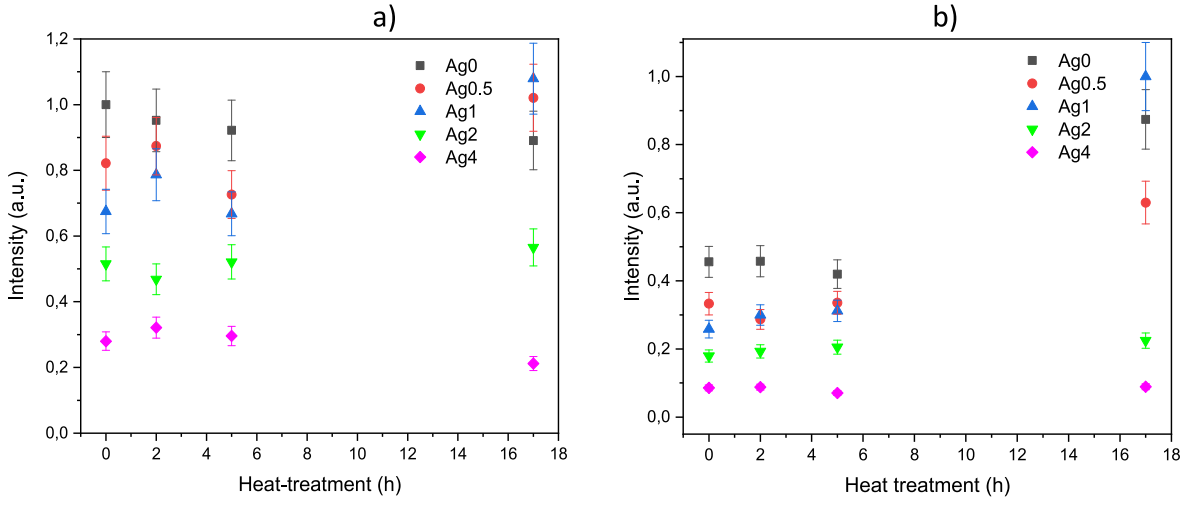

Fig. 4. Intensity of the emission at 2722 (a) and 670 nm (b) as a function of Ag_2O content prior to and after heat treatment at T_g + 20 °C for 2–17 h.

peak position is slightly different from those of the standard pattern of the Bi_4TeO_8 crystal, the difference being larger as the Ag_2O content increases. This shift in the peak position might indicate contraction in the structure of the crystals due to the substitution of the trivalent Bi by Ag, Te being tetravalent.

It is important to note that the glasses heat treated for 2 and 5 h are transparent GCs. The crystallite size was calculated using Scherrer equation [33] and is expected to be ~51 nm, independently of the glass composition and of the heat treatment duration. The crystallization of the glasses occurring during the heat treatment is also evidenced by the decrease in the transmittance properties of the glasses after the thermal treatment as depicted in Fig. 5b and c, which show the transmission

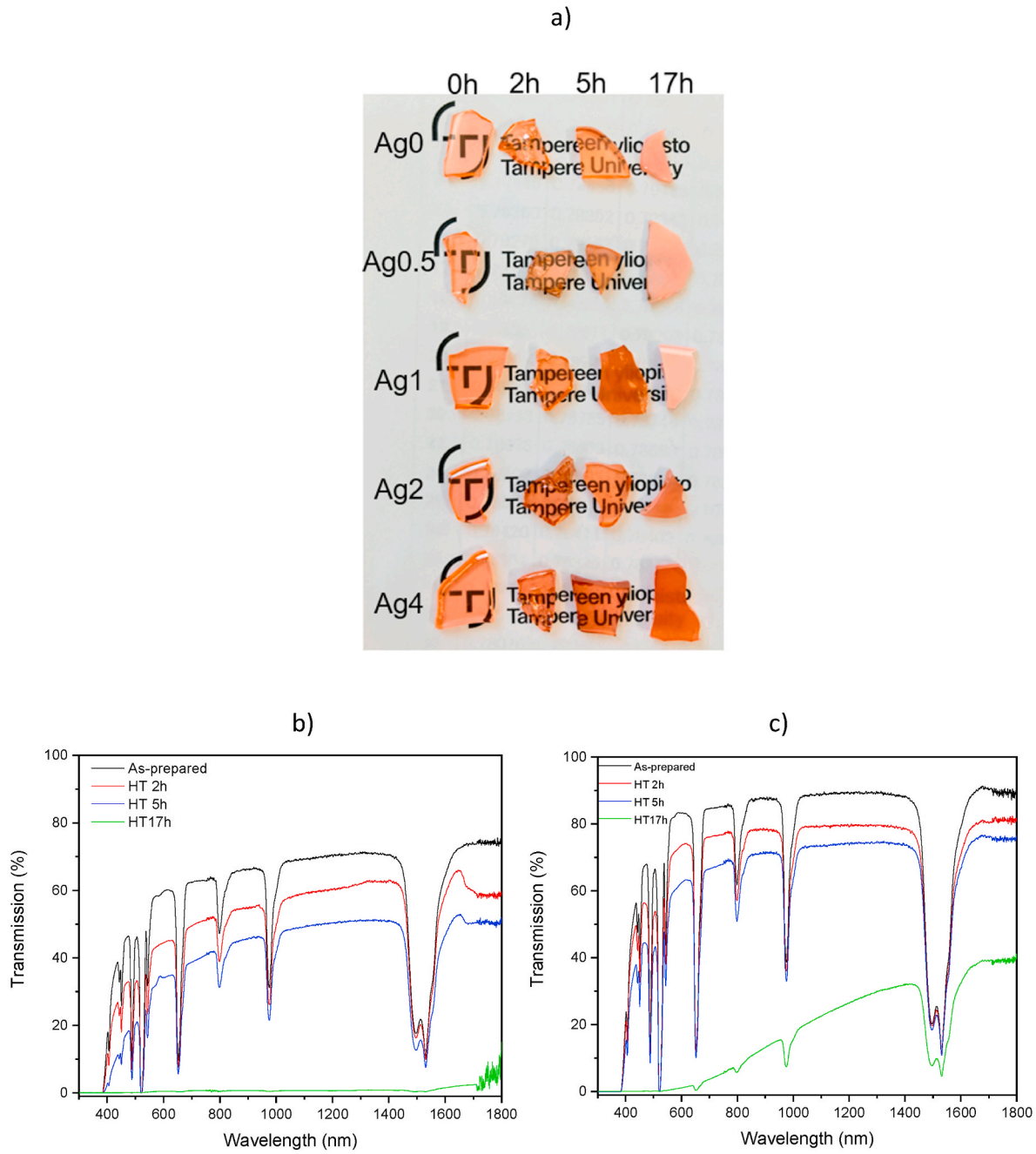

Fig. 5. Photographs of the glasses prior to and after heat treatment at (T_g + 20 °C) for 2–17 h (a) and transmission spectrum of the Ag0 (b) and Ag4 (c) glasses prior to and after heat treatment at (T_g + 20 °C) for 2–17 h (thickness of the glasses was 2.2 mm).

spectra of the as prepared and heat treated Ag0 and Ag4 glasses, taken as examples. The volume precipitation of the Bi_4TeO_8 crystals leads to light scattering [34]. The different transmission properties of Ag0 and Ag4 can be explained by the different refractive indices of the glasses: the high optical transmission of the Ag4 is due to its low refractive index compared to Ag0. Surprisingly, no band related to the SPR of Ag can be seen in the 400–500 nm range (Fig. 7) although nucleation of silver in tellurite using thermal treatment has been demonstrated in various tellurite glasses [35–37] and was evidenced with the appearance of an absorption band at ~400 nm [24].

The presence of crystals in the volume of the heat-treated glasses was confirmed using optical microscopy. Crystals with a square shape and with an average size of 15 μm were seen in the volume of all the heat-treated glasses (Fig. 8a taken Ag4 sample as an example). Similar crystals were reported by Massera et al. in undoped tellurite glasses within similar glass system [18]. TEM was also used to image the samples. As shown in Fig. 8b and c, dark dots of different sizes can be seen only in the TEM image of the Ag4 glass after 17 h at (T_g + 20 °C). According to the composition analysis, these spots are suspected to be isolated Ag NPs. These NPs have various shapes and sizes ranging between 25 and 42 nm. These Ag nanoparticles are expected to contribute to the light scattering and so to the losses in the transmittance properties seen in Fig. 5c. As compared to other studies focused on the precipitation of Ag NPs in tellurite glass [38,39], the resulting Ag NPs found in the investigated glasses are large and their spatial distribution poor. Similar observation was reported in Ag-containing tellurite glasses in TeO_2–ZnO system [40].

NLO microscopy, a powerful nondestructive imaging technique to

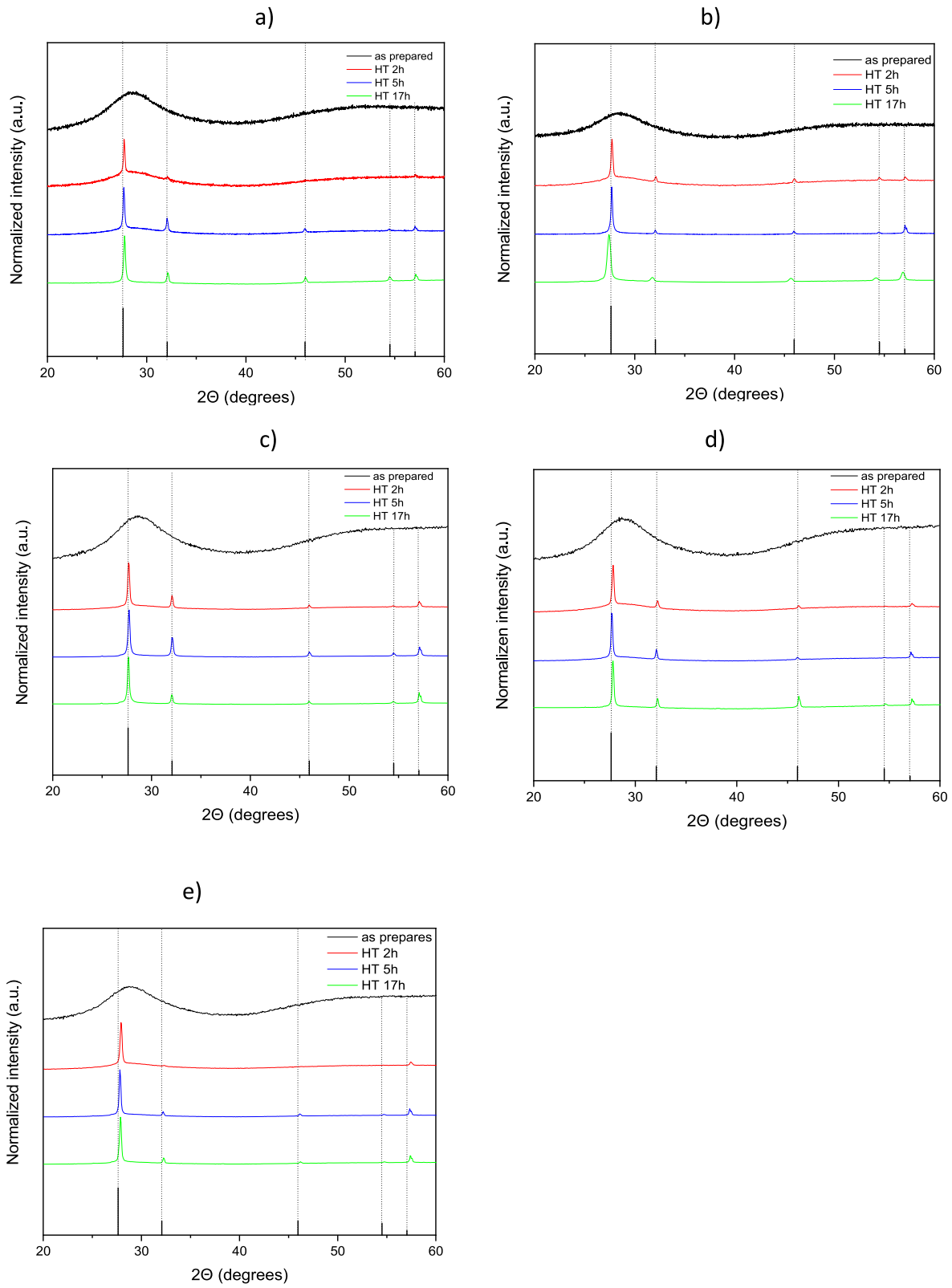

Fig. 6. XRD pattern of the Ag0 (a), Ag0.5 (b), Ag1 (c), Ag2 (d) and Ag4 (e) glasses prior to and after heat treatment at (T_g + 20 °C) for 2–17 h and the standard XRD pattern of the Bi_4TeO_8 crystal (ICDD 00-024-0157).

study a variety of nanostructures [41–43], was also used to study the GCs in this work. We first present the results of NLO microscopy of the Ag0 glass heat treated at (T_g + 20 °C) for 17 h. Shown in Fig. 9a is a crystal found inside the glass. As depicted in Fig. 9b–g, the nonlinear scattering signals inside the crystal are only found at the expected third-harmonic generation (Fig. 9c) and second-harmonic generation (Fig. 9f) wavelengths. These NLO signals are distinct from the background and almost vanish (about 60 counts per second (cps)) when the same region of interest is scanned in combination with different band-pass filters. We associate these hotspots to possible defects and

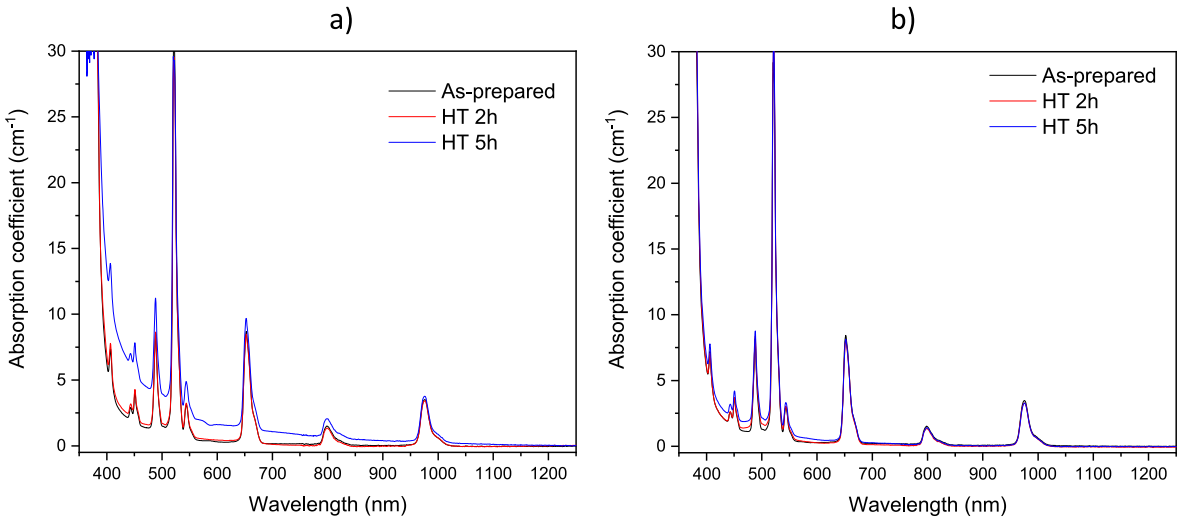

Fig. 7. Absorption spectra of the Ag0 (a) and Ag4 (b) glasses prior to and after heat treatment at (T_g + 20 °C) for 2 and 5 h.

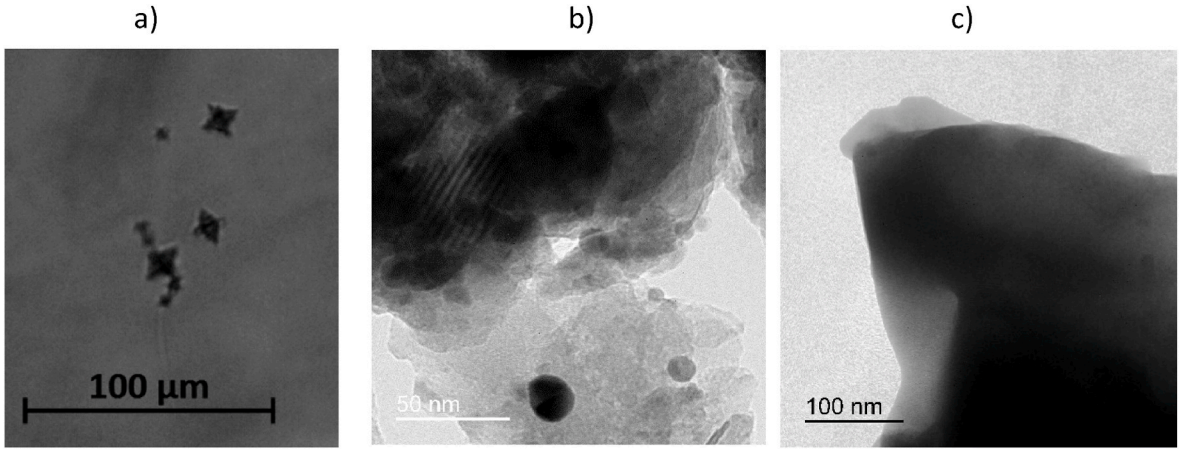

Fig. 8. Optical image of crystals found in glasses, taken the Ag4 glass heat treated at (T_g + 20 °C) for 17 h as example (10 × objective) (a), TEM images of the Ag4 (b) and Ag0 (c) glass heat treated at (T_g + 20 °C) for 17 h.

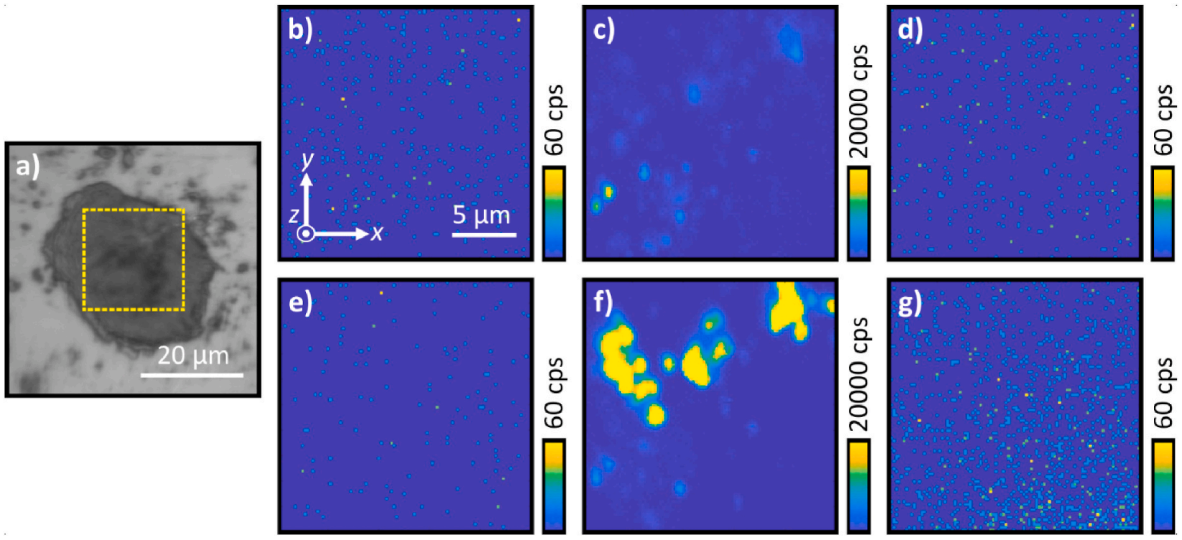

Fig. 9. Brightfield microscopy image (a) of the crystals in the Ag0 glass heat treated at (T_g + 20 °C) for 17 h. Corresponding transversal *xy* NLO scanning maps (b–f) of the marked region in (a) taken with different bandpass filters: 320 ± 20 nm (b), 356 ± 15 nm (c), 385 ± 13 nm (d), 500 ± 7.5 nm (e), 532 ± 9 nm (f) and 560 ± 7 nm (g). Comparative levels of the NLO signals are depicted in counts per seconds (cps).

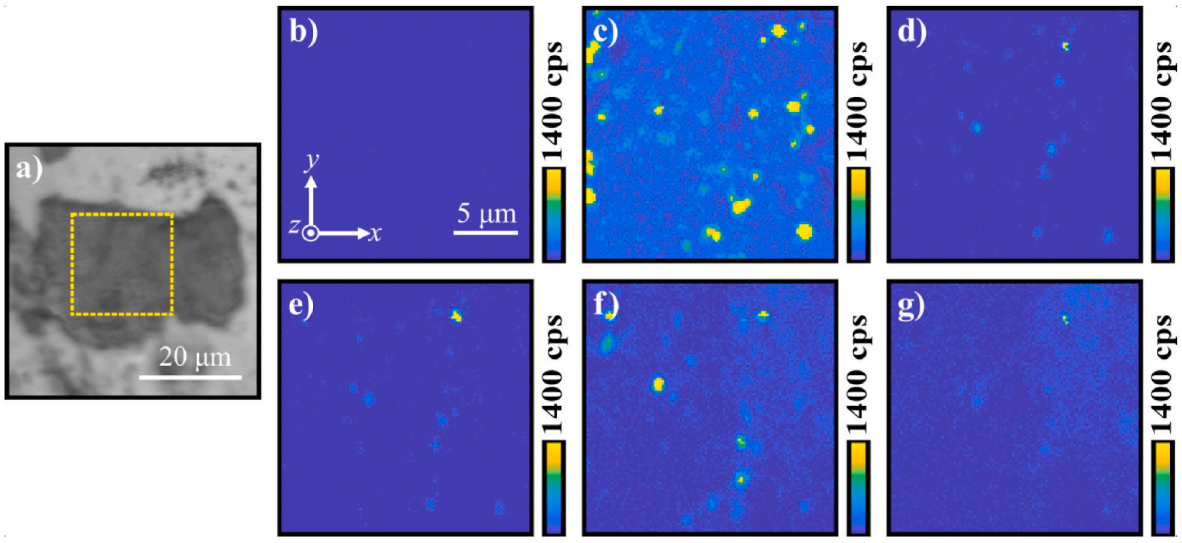

Fig. 10. Brightfield microscopy image (a) of the crystals in the Ag4 glass heat treated at (T_g + 20 °C) for 17 h. Corresponding transversal *xy* NLO scanning maps (b–f) of the marked region in (a) taken with different bandpass filters: 320 ± 20 nm (b), 356 ± 15 nm (c), 385 ± 13 nm (d), 500 ± 7.5 nm (e), 532 ± 9 nm (f) and 560 ± 7 nm (g). Comparative levels of the NLO signals are depicted in cps.

inhomogeneities inside the crystal, which makes the third-harmonic generation and second-harmonic generation both electric-dipole allowed and detectable in the far-field. In contrast, the NLO scans of a region in the Ag4 sample heat treated at (T_g + 20 °C) for 17 h (Fig. 10a) show the presence of micron-sized hotspots that stand out from the background. Importantly, the hotspots look almost qualitatively similar and appear in many spectral bands (Fig. 10b–g) suggesting the presence of nonlinear luminescence from subwavelength-sized Ag NPs in the glass sample when excited by femtosecond laser pulses. Here, the strongly confined fields near the vicinity of the metal nanostructures (through SPR) play a major role in the efficiency of the nonlinear luminescence [44]. In addition, the NLO scans at the expected third-harmonic generation (Fig. 10c) and second-harmonic generation (Fig. 10f) wavelengths exhibit NLO signals that are a little stronger than those detected away from the expected harmonic generation wavelengths. Inspection of the NLO data further showed that the THG signals from the Ag NPs are higher than their SHG signals by a factor of 7 as averaged from 10 NPs. The THG from plasmonic NPs originates mainly from bulk effects and at the vicinity of interfaces [45]. Although the SHG from the plasmonic NPs is well-known to exhibit a quadrupolar symmetry (i.e., non-radiative), the SHG from the NPs is expected to be boosted by the combined effects of symmetry breaking at surfaces, SPRs and local field asymmetries [46,47]. Altogether, these findings suggest that the SPR of the individual Ag NP is clearly influencing the local field distribution that drives the nonlinear response of the Ag NP [48]. In a similar context, our findings are in line and support previous observations of NLO enhancements in tellurite glasses [49] especially those imbued with NPs [50,51].

Although crystallization occurs with the precipitation of Ag NPs, no changes in the shape nor in the intensity of the absorption bands centered at 980 nm and 1.5 μm were measured after the heat treatment. The intensity and shape of the emission band centered at 1.5 μm remain also similar after heat treatment. While the shape of the (red and green) UC and MIR emissions remain unchanged after the heat treatment, the intensity of these emissions from the low Ag_2O concentrated glasses (x < 1) increases slightly after more than 5 h at T_g + 20 °C (Fig. 4a and b), the increase in the MIR emission being smaller than the increase in the (green and red) UC emissions. It should be noted the Ag0.5 glass-ceramic has slightly lower UC emission than the Ag0 and Ag1 glass-ceramics for reason which is not fully understood. Considering the uncertainty of the measurement, we suspect the Ag0, Ag0.5 and Ag1 glass-ceramics to have similar intensity of (green and red) UC emissions. When x > 2, no changes in the intensity of the UC, NIR and MIR emissions were measured within 10%. Therefore, based on the spectroscopic properties of the GCs, the local electric field is thought to remain similar after heat treatment and so the sites of Er^{3+} ions. The Er^{3+} ions are suspected to remain in the amorphous part of the glass-ceramics. The amount of Ag NPs is probably too small to have an impact on the spectroscopic properties of the glasses. When excited at 980 nm, the Er^{3+} ions are excited to the $^4I_{11/2}$ level. From this level, the ions can relax to $^4I_{13/2}$ level emitting the MIR fluorescence and then to $^4I_{15/2}$ level emitting the NIR fluorescence. The generation of the visible emissions can be benefited from the $^4I_{13/2} + {}^4I_{13/2} \rightarrow {}^4I_{9/2} + {}^4I_{15/2}$ and $^4I_{11/2} + {}^4I_{11/2} \rightarrow {}^4F_{7/2} + {}^4I_{15/2}$ process increasing the population of the upper $^4I_{9/2}$ level which relaxes to$^4I_{11/2}$ level as suggested in Ref. [31]. As a consequence, the population of the first excited level is thus expected to be reduced as the $^4I_{13/2}$ level is populated from $^4I_{11/2}$ by non-radiative relaxation when using 980 nm pumping. Therefore, we suspect the increase in the UC and MIR emissions observed from the glasses with x < 1 after the thermal treatment to be related to the decrease in the Er–Er distances which can be induced by the precipitation of the Bi_4TeO_8 crystal. One should note that a decrease in the intensity of the NIR emission is expected as ETU between Er^{3+} ions is expected to reduce the population in the $^4I_{13/2}$ level [31]. However, the decrease is probably too small to be detected. As no changes in the intensity of the UC, NIR and MIR emissions are seen from the glasses with x > 2, the crystallization has no impact on the Er–Er distances in these glasses. It is possible that the precipitation of the Bi_4TeO_8 crystal has no impact on the Er–Er distances in depolymerized network (glasses with x > 2) whereas it decreases the Er–Er distances in polymerized network (glasses with x < 2).

4. Conclusion

Er^{3+} doped glasses within the TeO_2–ZnO–Bi_2O_3–Ag_2O system were prepared using standard melting process. Although the introduction of Ag_2O leads to the depolymerization of the tellurite network, it has no impact on the site of the Er^{3+} ions but it increases the Er–Er distances leading to a decrease in the intensity of the green and red UC emissions. It is shown here that a heat treatment of the glasses above T_g for a few hours is enough to grow Bi_4TeO_8 crystal in the volume of the glass as confirmed by XRD and an optical microscope. Although Ag nanoparticles could be seen in the heat treated glass using TEM and NLO imaging, no SPR band of Ag could be seen in the absorption spectra of the glasses. From the spectroscopic properties of the glass, the crystals

appear to be Er^{3+} free. The precipitation of the Bi_4TeO_8 crystal in the low Ag_2O concentrated glass allows to increase the intensity of the UC and MIR emissions indicating that the glass-ceramics prepared with <1 mol% of Ag_2O are promising materials.

Credit author statement

L.P. conceived and designed this work. IA, IS, RP and LP prepared and characterized the glasses. SA and GB carried out the measurement of the nonlinear optical images while AO and HE focused on the TEM images. All authors discussed the results and contributed to the writing of the manuscript.

Declaration of competing interest

The authors declare that they have no known competing financial interests or personal relationships that could have appeared to influence the work reported in this paper.

Acknowledgment

Academy of Finland (Flagship Programme, Photonics Research and Innovation PREIN-320165 and Academy Project -326418), Pirkanmaa Regional Fund and Magnus Ehrnrooth foundation are greatly acknowledged for the financial support. S.A. is grateful to Jenny and Antti Wihuri Foundation for financial support.

References

[1] J.S. Wang, E.M. Vogel, E. Snitzer, Tellurite glass: a new candidate for fiber devices, Opt. Mater. 3 (1994) 187–203.
[2] A. Mori, Y. Ohishi, M. Yamada, H. Ono, S. Sudo, 1.5 μm Broadband Amplification by Tellurite-Based EDFAs, Optical Fiber Conference, Washington, USA, 1997. PD-1, 1997.
[3] R. El-Mallawany, Tellurite glasses: part 1. Elastic properties, Mater. Chem. Phys. 53 (1998) 93–120.
[4] Y. Wang, J. Ohwaki, New transparent vitroceramics codoped with Er^{3+} and Yb^{3+} for efficient frequency upconversion, Appl. Phys. Lett. 63 (1993) 3268–3270.
[5] Y. Ohishi, A. Mori, M. Yamada, H. Ono, Y. Nishida, K. Oikawa, Gain characteristics of tellurite-based erbium-doped fiber amplifiers for 1.5-μm broadband amplification, Opt. Lett. 23 (4) (1998) 274.
[6] F. Vetrone, J.C. Boyer, J.A. Capobianco, A. Speghini, M. Bettinelli, 980 nm excited upconversion in an Er-doped ZnO–TeO_2 glass, Appl. Phys. Lett. 80 (2002) 1752–1754.
[7] A.A. Assadi, K. Damak, R. Lachheb, A. Herrmann, E. Yousef, C. Rüssel, R. Maâlej, Spectroscopic and luminescence characteristics of erbium doped TNZL glass for lasing materials, J. Alloys Compd. 620 (2015) 129–136.
[8] V.A.G. Rivera, S.P.A. Osorio, Y. Ledemi, D. Manzani, Y. Messaddeq, L.A.O. Nunes, E. Marega Jr., Localized surface plasmon resonance interaction with Er^{3+}-doped tellurite glass, Opt. Express 18 (2010) 25321–25328.
[9] H. Fares, H. Elhouichet, B. Gelloz, M. Férid, Silver nanoparticles enhanced luminescence properties of Er^{3+} doped tellurite glasses: effect of heat treatment, J. Appl. Phys. 116 (2014) 123504-1–123504-10.
[10] S.D. Stookey, Method of making ceramics and products thereof, US Patent 2 (1960) 920–971.
[11] R. J. Deubener, M. Allix, M.J. Davis, A. Duran, T. Höche, T. Honma, T. Komatsu, S. Krüger, I. Mitra, R. Müller, S. Nakanei, M.J. Pascuald, J.W.P. Schmelzerj, E. D. Zanottok, S. Zhoul, Updated definition of glass-ceramics J. Non-Cryst. Solids 501 (2018) 3–10.
[12] G.H. Beall, D.A. Duke, Transparent glass-ceramics, J. Mater. Sci. 4 (1969) 340–352.
[13] R.W. Hopper, Stochastic theory of scattering from idealized spinodal structures: II. Scattering in general and for the basic late stage model, J. Non-Cryst. Solids 70 (1985) 111–142.
[14] K. Shioya, T. Komatsu, H.G. Kim, R. Sato, K. Matusita, Optical properties of transparent glass-ceramics in K_2O-Nb_2O_5-TeO_2 glasses, J. Non-Cryst. Solids 189 (1995) 16–24.
[15] D.M. da Silva, L.R.P. Kassab, S.R. Lüthi, C.B. de Araújo, A.S.I. Gomes, M.J.V. Bell, Frequency upconversion in Er^{3+} doped PbO–GeO_2 glasses containing metallic nanoparticles, Appl. Phys. Lett. 90 (2007) 081913-1–081913-3.
[16] C. Yu, J. Zhang, L. Wen, Z. Jiang, New transparent Er^{3+}-doped oxyfluoride tellurite glass ceramic with improved near infrared and up-conversion fluorescence properties, Mater. Lett. 61 (2007) 3644–3646.
[17] Y. Zhang, H. Lei, G. Li, L. Zeng, J. Tang, Yb^{3+}/Er^{3+} co-doped transparent tellurite glass-ceramic for enhanced upconversion luminescence, Opt. Mater. 99 (2020) 109552-1–109552-7.
[18] J. Massera, J. Remond, J. Musgraves, M. Davis, S. Misture, L. Petit, K. Richardson, Nucleation and growth behavior of glasses in the TeO_2-Bi_2O_3-ZnO glass system, J. Non-Cryst. Solids 356 (2010) 2947–2955.
[19] B. Tatian B, Fitting refractive-index data with the Sellmeier dispersion formula, Appl. Opt. 23 (1984) 4477–4485.
[20] M. Çelikbilek, A.E. Ersundu, N. Solak, S. Aydin, Thermal and microstructural investigation of the TeO_2-WO_3 system, J. Alloys Compd. 509 (2011) 5646–5654.
[21] R.J. Amjad, M.R. Sarah, M. R Dousti, S.K. Ghoshal, M.N.A. Jamaludin, Surface enhanced Raman Scattering and plasmon enhanced fluorescence in zinc-tellurite glass, Opt. Express 21 (2013) 14282–14290.
[22] A.A. Kharlamov, R.M. Almeida, J. Heo, J. Vibrational spectra and structure of heavy metal oxide glasses, J. Non-Cryst. Solids 202 (1996) 233–240.
[23] G. Guery, A. Fargues, T. Cardinal, M. Dussauze, F. Adamietz, V. Rodriguez, J. D. Musgraves, K. Richardson, P. Thomas, Impact of tellurite-based glass structure on Raman gain, Chem. Phys. Lett. 554 (2012) 123–127.
[24] A. Bachvarova-Nedelcheva, R. Iordanova, K.L. Kostov, Synthesis, structure and properties of silver tellurite glasses, Mater. Res. Express 6 (2019) 125202, 125202.
[25] X. Peng, F. Song, S. Jiang, N. Peyghambarian, M. Kuwata-Gonokami, L. Xu, Fiber-taper-coupled L-band Er^{3+}-doped tellurite glass microsphere laser, Appl. Phys. Lett. 82 (2003) 1497.
[26] S. Shen, A. Jha, E. Zhang, S.J. Wilson, Compositional effects and spectroscopy of rare earths (Er^{3+}, Tm^{3+}, and Nd^{3+}) in tellurite glasses, Compt. Rendus Chem. 5 (2002) 921–938.
[27] S.-H. Kim, T. Yoko, S. Sakka, Linear and nonlinear optical properties of TeO_2 glass, J. Am. Ceram. Soc. 76 (1993) 2486–2490.
[28] R. El-Mallawany, R.D. Abdalla, I.A. Ahmed, New tellurite glasses: optical properties, Mater. Chem. Phys. 109 (2008) 291–296.
[29] G. Dai, F. Tassone, A. LiBassi, V. Russo, C.E. Bottani, F. D'Amore, TeO_2-based glasses containing Nb_2O_5, TiO_2, and WO_3 for discrete Raman fiber amplification, IEEE Photon. Technol. Lett. 16 (2004) 1011–1013.
[30] H. Ohkawa, H. Hayashi, Y. Kondo, Influence of water on non-radiative decay of Yb^{3+}–$^2F_{5/2}$ level in phosphate glass, Opt. Mater. 33 (2) (2010) 128–130.
[31] Y. Liu, X.Y. Liu, W.C. Wang, W.J. Zhang, Q.Y. Zhang, 2.7 μm emission in Er^{3+} doped glass ceramics containing lutetium oxyfluoride nanocrystals, Opt. Mater. Express 6 (9) (2016) 2759.
[32] A. Gonçalves, V.S. Zanuto, G.A.S. Flizikowski, A.N. Medina, F.L. Hegeto, A. Somer, J.L. Gomes Jr., J.V. Gunha, G.K. Cruz, C. Jacinto, N.G.C. Astrath, A. Novatski, Luminescence and upconversion processes in Er^{3+}-doped tellurite glasses, J. Lumin. 201 (2018) 110–114.
[33] U. Holzwarth, N. Gibson, The Scherrer equation versus the "Debye-Scherrer equation, Nat. Nanotechnol. 6 (2011) 534.
[34] P.A. Tick, N.F. Borrelli, I.M. Reaney, The relationship between structure and transparency in glass-ceramic materials, Opt. Mater. 15 (2000) 81–91.
[35] L.R.P. Kassab, L.F. Freitas, T.A.A. de Assumpção, D.M. da Silva, C.B. de Araújo, Frequency upconversion properties of Ag: TeO_2–ZnO nanocomposites codoped with Yb^{3+} and Tm^{3+} ions, Appl. Phys. B Laser Opt. 104 (2011) 1029.
[36] V.D. Del Cacho, A.L. Siarkowsi, N. Morimoto, H.V. Borges, L.R.P. Kassab, Fabrication and characterization of TeO_2-ZnO rib waveguides, ECS Trans. 31 (2010) 219.
[37] T.A.A. de Assumpção, M.E. Camilo, L.R.P. Kassab, A.S.L. Gomes, C.B. de Araújo, N. U. Wetter, Frequency upconversion properties of Tm^{3+} doped TeO_2–ZnO glasses containing silver nanoparticles, J. Alloys Compd. 536 (2012) S504.
[38] G.H. Silva, D.P.A. Holgado, V. Anjos, M.J.V. Bell, L.R.P. Kassab, C.T. Amâncio, Richard Moncorg, Effect of Ag nanoparticles on the radiative properties of tellurite glasses doped with Er^{3+}, Yb^{3+} and Tm^{3+} ions, Opt. Mater. 37 (2014) 281–286.
[39] B. Huang, Y. Zhou, F. Yang, L. Wu, Y. Qi, J. Li, The 1.53 μm spectroscopic properties of Er^{3+}/Ce^{3+}/Yb^{3+} tri-doped tellurite glasses containing silver nanoparticles, Opt. Mater. 51 (2016) 9–17.
[40] T.A.A. de Assumpcão, D.M. da Silva, M.E. Camilo, L.R.P. Kassab, A.S.L. Gomes, C. B. de Araújo, N.U. Wetter, Frequency upconversion properties of Tm^{3+} doped TeO_2–ZnO glasses containing silver nanoparticles, J. Alloys Compd. 536S (2012) S504–S506.
[41] G. Bautista, L. Kallioniemi, L. Petit, Unveiling structured domains of persistent luminescent microparticles using second-harmonic generation microscopy, Opt. Express 28 (18) (2020) 25858–25868.
[42] C. Dreser, D.A. Gollmer, G. Bautista, X. Zang, D.P. Kern, M. Kauranen, M. Fleischer, Plasmonic mode conversion in individual tilted 3D nanostructures, Nanoscale 11 (12) (2019) 5429–5440.
[43] R. Camacho-Morales, G. Bautista, X. Zang, L. Xu, L. Turquet, A. Miroshnichenko, H. H. Tan, A. Lamprianidis, M. Rahmani, C. Jagadish, D.N. Neshev, M. Kauranen, Resonant harmonic generation in AlGaAs nanoantennas probed by cylindrical vector beams, Nanoscale 11 (4) (2019) 1745–1753.

[44] M.R. Beversluis, A. Bouhelier, L. Novotny, Continuum generation from single gold nanostructures through near-field mediated intraband transitions, Phys. Rev. B 68 (2003) 115433-1–115433-10.
[45] M. Lippitz, M.V. van Dijk, M. Orrit, Third-harmonic generation from single gold nanoparticles, Nano Lett. 5 (4) (2005) 799–802.
[46] J. Butet, P.-F. Brevet, O.J.F. Martin, Optical second harmonic generation in plasmonic nanostructures: from fundamental principles to advanced applications, ACS Nano 9 (11) (2015) 10545–10562.
[47] B.K. Canfield, H. Husu, J. Laukkanen, B. Bai, M. Kuittinen, J. Turunen, M. Kauranen, Local field asymmetry drives second-harmonic generation in noncentrosymmetric nanodimers, Nano Lett. 7 (5) (2007) 1251–1255.
[48] M. Kauranen, A. Zayats, Nonlinear plasmonics, Nat. Photonics 6 (2012) 737–748.
[49] S. Manning, H. Ebendorff-Heidepriem, T.M. Monro, Ternary tellurite glasses for the fabrication of nonlinear optical fibres, Opt. Mater. Express 2 (2) (2012) 140–152.
[50] C. Lasbrugnas, P. Thomas, O. Masson, J.C. Champarnaud-Mesjard, E. Fargin, V. Rodriguez, M. Lahaye, Second harmonic generation in poled tungsten tellurite glasses, in: Society of Glass Technology, vol. 31, Glass Technology, 2009, pp. 775–780, 6.
[51] N.T. Lo, H.N. Nguyen, N.L. Dao, M.S. Hoang, Combination of nonlinear optical properties in thermally poled germanotellurite glass-ceramics, Int. J. Appl. Glass Sci. 13 (2022) 235–243.